ISBN: 978-3-95450-207-3 doi:10.18429/JACoW-MEDSI2018-WEOPMA07

DEVELOPMENT OF A NEW SUB-4K ARPES ENDSTATION AT PSI

D. Trutmann*, S. Maag, L. Nue, A. Pfister, A. Schwarb, K. Zehnder, S. Hasanaj, M. Shi, N. C. Plumb
Paul Scherrer Institut (PSI), 5232 Villigen PSI, Switzerland

Abstract

In spring 2016 a project was started to renew the high-resolution ARPES endstation of the Surface/Interface Spectroscopy (SIS) beamline at PSI. The focus lay on achieving sample temperatures below 4 K while maintaining 6 degrees of freedom.

This made it necessary to redesign all thermally active parts, such as the connection to the cryostat, the flexible braid that enables the tilt and azimuthal movement, the sample clamping as well as the thermal isolators that hold the clamping device in place. A newly introduced shield in the main analyser chamber, cooled by separate cryopumps, is used to remove nearly all radiation heat load.

A major milestone has recently been taken, by running cryogenic tests on a test stand. The simplified setup reached sample temperatures of 3.35 K. The temperature loss from the cryostat to the sample was as low as 0.6 K. Encouraged by these results, it is believed that the final endstation will be able to reach temperatures even below 3 K. With the new cryo concept, the thermal performance seems to be mainly limited by the radiative heat load emitted by the analyser lens.

The new endstation is planned to be in operation by spring 2019.

INTRODUCTION

Angle-resolved photoemission spectroscopy (ARPES) is a powerful technique to directly measure the electronic band structure and interactions in solids [1] that is widely employed at many synchrotrons. ARPES is primarily used to study materials at the cutting edge of condensed matter physics and solid state engineering. Practitioners in the field are generally interested in experimental systems that can reach ever-lower energy and temperature scales, as these provide access to many interesting, unstudied science cases and ideal conditions obtaining sharp spectra and discerning fine features.

Of course, the pursuit of lower temperature and better resolution always involves design tradeoffs. While the record lowest temperature for ARPES at a synchrotron currently is below 1 K using a He-3 cryostat [2], this level of performance is possible only by drastically reducing access to the sample in order to reduce the radiation load, which in turn introduces practical issues for sample handling, manipulation, alignment and data acquisition.

Considering the state-of-the-art in VUV beamlines – and, more importantly, the performance guarantees of commercially available ARPES analyzers – an optimistic estimate of the foreseeable best-case resolution at SIS beamline is about $\Delta E = 1$ meV. Equivalent thermal broadening occurs around $T \approx \Delta E/(4k_B) = 3$ K. Below roughly this point, we expect drastically diminishing scientific returns on any hard-fought improvements in the temperature. In light of the above, we have therefore conceived of the SIS upgrade as a new standard in high-throughput *workhorse* systems for ARPES at synchrotrons, with the goal of sub-4 K temperature performance and an optimistic design target of 2 K to 3 K.

GENERAL OVERVIEW

The current endstation offers a six degrees of freedom (DOF) mechanical system, with no coupling between any DOF and only a negligible thermal drift along on the azimuthal axis and no drift along all other DOF. It further offers an open environment such that sample manipulation and alignment is easy. Overall, these features gives it a very competitive all-around performance among ARPES manipulators. Apart from maintaining the above features, the new endstation, figure 1 and 2, should improve or introduce new features, such as:

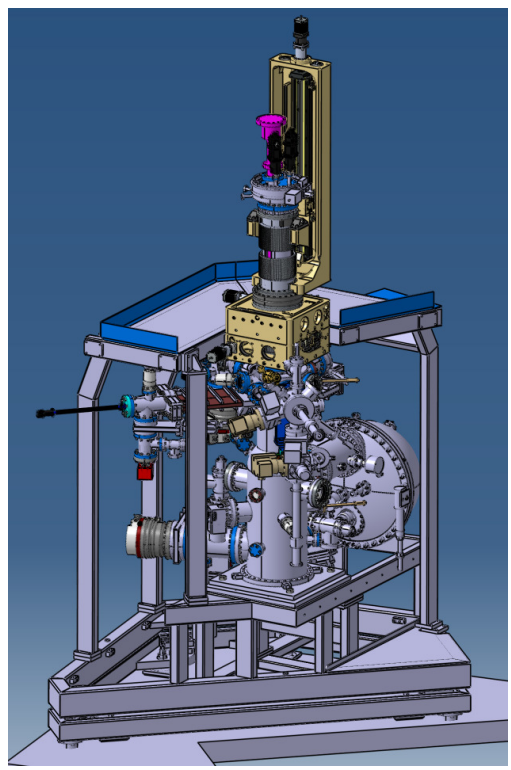

Figure 1: The current state of the new endstation.

- improved sample temperature from currently reachable 14 K (measured on the sample plate holder) to <4 K (measured on the sample plate itself)

* daniel.trutmann@psi.ch

ISBN: 978-3-95450-207-3 doi:10.18429/JACoW-MEDSI2018-WEOPMA07

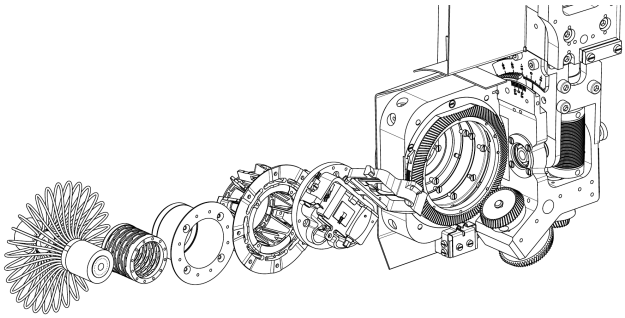

Figure 2: Disassembled manipulator head with (left to right) braid, isolator 1, shield, isolator 2, sample plate holder with shield, head support structure with tilt and azimuthal DOF.

- improved analyser resolution to <1.6 meV and adds a *deflection* scanning mode, which may be especially helpful for small samples
- improved vacuum to below 10^{-11} mbar
- switch from custom sample plates to Omicron-compatible sample plates
- introduce a way to recover sample pieces that fell down in the preparation chamber (PC)

CRYOGENIC DEVELOPMENT

The cryogenic conductors, isolators and their interfaces are designed with great care to avoid any unwanted temperature drop. Overall, every cryogenic part has the potential for causing a critical temperature loss such that the design target can be missed. The whole cooling chain, starting from the liquid helium inside the cryostat all the way to the sample plate itself was optimised for optimal heat transfer. Figure 3 gives a topological overview.

Thermal radiation onto the sample is mainly blocked through the AC-cryoshield, the analyser *nose cone* and the sample holder shield. Other *onboard* shields, directly mounted onto the cryostat, removes thermal radiation from the manipulator support structure. Among all warm parts, only the analyser lens has a direct line-of-sight with the sample. The heat load on the sample due to radiation is estimated to be approximately 5 mW.[1] Conductive heat load onto the sample plate holder, through *Isolator 1* (figure 3), is estimated to be below 1 mW. This is supported by Finite Element Anaysis (FEA)[2,3] and conducted tests on a modified test setup.

Braid

The braid must be flexible enough to do the relative motion of the tilt and azimuth DOF, but at the same time, it must have a large enough crosssection to reduce the temperature loss between both ends. Several trials, that mainly

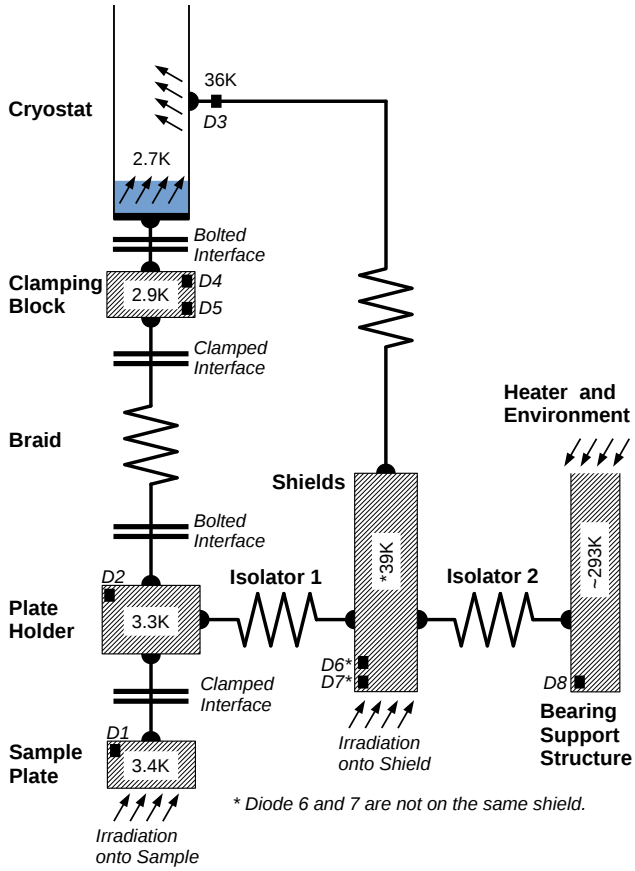

Figure 3: Simplified topological cryo-layout.

differ in the way how the strain-ends are clamped, have been developed and manufactured. In one of the first designs, shown in figure 4a, the braids were compressed by applying a radial force. Cut-ups showed that the contact between the wires and the deformed jacket is poor, figure 4b and 4c. Overall the result was not satisfactory, as an unacceptable large temperature loss across the braid was expected.

As a consequence, a new design was developed that pressed the wires between an outer and an inner cone in order to optimise the resulting contacts. Furthermore, the ends were welded using electron beam welding and later vacuum-annealed, see figure 5c. Deformation from pressing made it necessary to machine the braid ends. Cutups showed indeed that the connection between the single wires and the end-piece is very good, figure 5a and 5b. It can however not be determined what contributed more to the good conductivity that has later been observed in the tests, the pressing or the welding.

Plate Holder

Thermal contact conductance is the ability to transport heat from one body across a contact interface to another body. It depends on the force [3] with which both bodies are pressed together, but somewhat counter-intuitively, not on the area and hence not on the pressure (force per area). The temperature gradient across an interface exists, because sur-

[1] Based on the exposed sample plate (D = 10 mm) and lens (D = 30 mm), located in 34 mm distance.
[2] Thermal conductivity for copper (OFE): [5] and [6]
[3] Thermal conductivity for Vespel SP1: [5] and [7]

ISBN: 978-3-95450-207-3 doi:10.18429/JACoW-MEDSI2018-WEOPMA07

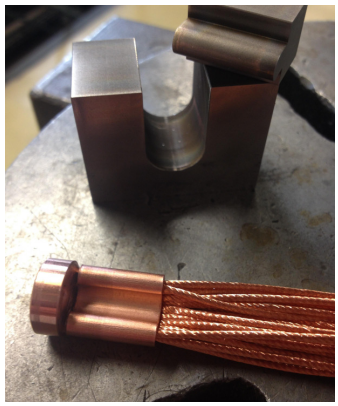

(a) Photo of the pressed braid-end and the pressing tool

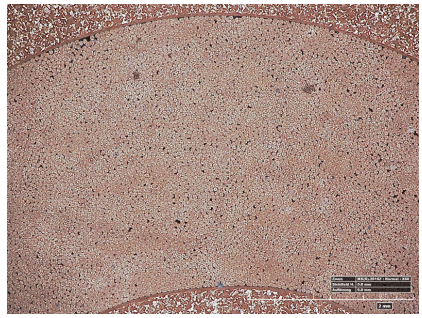

(b) Picture of a cut-up, showing the middle of the croissant-shaped cross section. Towards the very left and right end of the cut, the number of gaps increases severely.

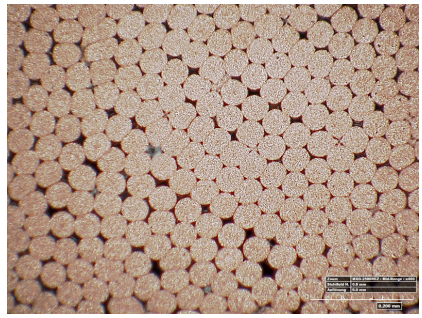

(c) Magnified view of a central area, in the middle of the cross section. This situation is about average for such locations. The single wires have a diameter of 0.05 mm.

Figure 4: Early braid design.

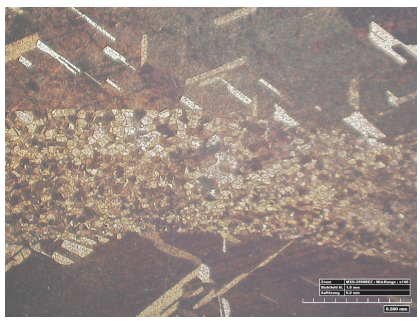

(a) The lower part shows the inner cone, the upper part the outer counterpart. In between are the wires, which run perpendicular to the paper.

(b) Detail of the single wires, which have been deformed to hexagons. The single wires have a diameter of 0.05 mm.

(c) Axial cross section along the single braids. The braids comes from the left and enters the welding seam on the right.

Figure 5: Iterated braid design.

faces are not perfectly flat but instead have a hilly topology. Therefore, two surfaces that are in contact touch each other only on a small number of places. As the pressing force increases, small deformations occur and causes the number of contact spots and their sizes to increase, followed by an improved thermal contact conductance [4]. The thermal contact conductance is material, temperature and surface-quality specific.

Using experimental data presented in [3], it was possible to derive a *force-to-temperature-drop* diagram, such that the expected loss across the *sample plate – holder* interface could be estimated. The resulting graph, figure 6, is however not universally applicable since it is constructed for this specific use. As a consequence, it became clear that the sample plate holder must be able to clamp a sample plate with kN's of clamping force.

Several designs have been considered, such as a design based on flat springs and a design using a *car jack*-like flexure. The first was dismissed due to the limited force delivered (twice 350 N to 550 N, cause a temperature drop of 0.7 K to 1 K), while the second was rejected due to the very small travelling distance of the *jack* when the angles

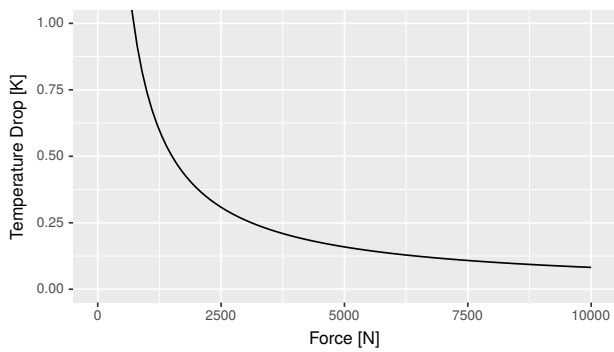

Figure 6: Force dependent temperature drop estimated for the sample plate – holder interface.

of were set appropriately such that the force was sufficiently high.

It became clear that none of these mechanisms would suffice. Instead a design using a worm-gear, a fine pitch thread and a wedge/ram pair was pursued, figure 7. While the torque of the wobblestick used to operate the holder is limited to 0.4 Nm, it is possible to see the holder (elastic)

ISBN: 978-3-95450-207-3 doi:10.18429/JACoW-MEDSI2018-WEOPMA07

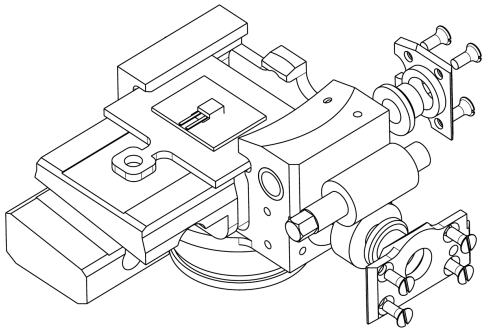

Figure 7: Final design of the sample plate holder.

deform with a torque even below 0.1 Nm. Based on this input torque (0.1 Nm), gear ratio and pitch as well as appropriate efficiencies for each mechanism, an estimated clamping force of 3.7 kN results, leading to a temperature drop of only 0.2 K.

Isolators

Experience from previous endstation upgrades and FEA investigations have shown, that better thermal decoupling is required. As the current endstation already uses an isolator that is on the edge of what manufacturing capabilities allows, an topological change was focused.

The new layout utilises two separate isolators, made of Vespel SP1, that are connected to the radiation shield in between, such that the temperature gradient across the rigid insulation assembly is in favour of the lowest temperature level. Furthermore, the thermal contraction of both isolators compensate each other, such that the overall thermal drift is expected to improve even further.

AC-Radiation Shield

The radiation heat load is essentially a function of the solid angle of the sample that is exposed to room temperature parts. The most significant portion of this load can be removed by a statically mounted shield inside of the AC chamber. While the manipulator support structure is shielded with on-board shields, cooled by the cryostat exhaust gas, the AC shield is cooled by a secondary cooling system also mounted onto the AC chamber. This allows to carry much of the shielding duty over from the cryostat to the secondary system. Meanwhile, this permanent radiation shielding in the AC chamber carries the side benefit of acting as a cryopump, thus enabling ARPES to be performed in an exceptionally clean environment.

The shield is composed of two main parts – an upper bell-shaped part that allows a good view onto the sample and manipulator through holes and cutouts and a second, bucket-like part that can be moved up such that it closes all unnecessary openings, see figure 8. The lifting is done by a vertical threaded shaft, driven by a wormgear that is coupled to a motor located outside of the AC.

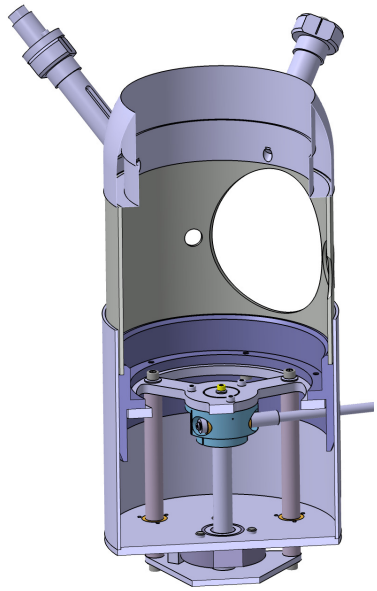

Figure 8: Stationary shield within the AC chamber.

CRYOTEST SETUP

To test the performance of the cryogenic parts, a test setup was build. It was mounted onto a CF150 flange, through which the cryostat reached down, parallel to a (room temperature) support bar. Figure 9 shows the lower parts of the setup in detail, without the outer shielding.

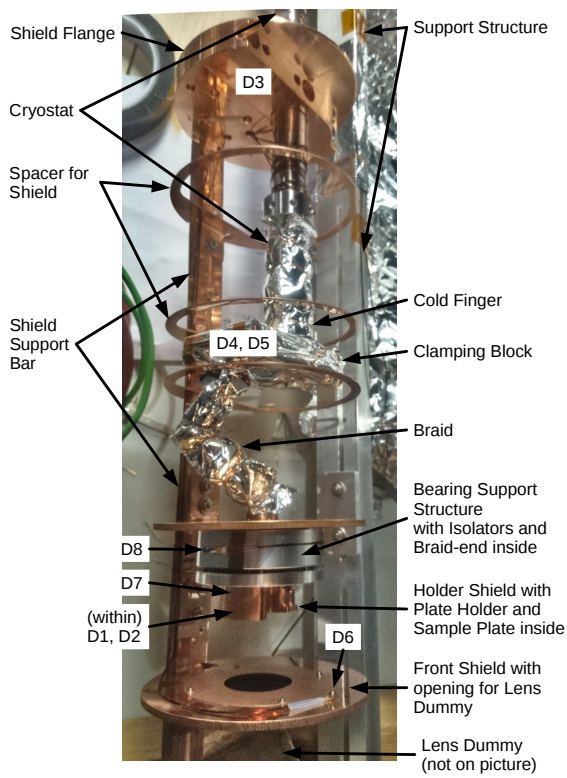

Figure 9: Test setup without the shield-wrapping. The lower part of the cryostat, the clamping block and the braid are wrapped in super insulating foil.

ISBN: 978-3-95450-207-3 doi:10.18429/JACoW-MEDSI2018-WEOPMA07

Support Bar

The support bar holds room temperature parts in place. It is equipped with a heater to counter the thermal radiation deficit caused by the cryogenic parts right next to it. At its lower end, a bent aluminium sheet mimed the analyser lens. The surface of the lens dummy was treated with rough grinding paper to ensure a rough and oxidised surface, such that the emissivity was sufficiently high. If further tests will be performed, it will be good to anodise this part, in order to better mimic the emissivity of the instrument. It is the main source of radiation into the cryogenic system.

A couple of centimetres above the lens dummy, the warm support bar connects to the *bearing dummy*. This part is a replacement for two ball bearings required for the azimuthal rotation. On its inner diameter, it holds the second isolator and thus the cryogenic assembly in place.

Shield

Approximately 250 mm above the cold finger a larger copper disk clamps onto the cryostat tube, *shield flange* in figure 9. On its outer diameter, a copper bar attaches and reaches down, parallel to the cryostat and the support bar. It supplies the intermediate temperature level to all shields. Approximately in the middle, a disk attaches that holds a cryoshield in place and supplies it with the shield temperature. At the lower end of the bar, another disk attaches with a hole in it, through which the lens dummy emits thermal radiation onto the sample. The complete assembly is wrapped within a thin copper sheet to protect it from the irradiation of the environment.

Cryogenic Chain

In comparison to the actual endstation, the cryogenic test setup only differs in how the braid is clamped onto the cryostat and the location of some shields. Overall the setup is the same and should perform as such. To be able to measure the temperature of the sample plate, without exposing the diode itself to the incoming irradiation, a specially designed, non-standard plate has been manufactured. While the plate has the overall shape of an Omicron plate, it has an additional extension to clamp a silicon diode on it, hidden from the incoming thermal radiation from the lens dummy.

MEASUREMENTS

Tests performed with this setup showed that the thermal design is sound. Figure 10 shows the development of the temperatures throughout the test, while the lowest stable operation point is also shown in figure 3. The diode within the cryostat was not recorded but used to adjust the helium flow. The helium consumption is within the same range as with the current endstation. During warmup, diode 1 (sample plate) seems to have made thermal contact with a shield.

ACKNOWLEDGEMENTS

A special thanks goes to the workshop crew for their quality work and flexibility.

This work is supported by the *Swiss National Science Foundation* project number 206021_164016.

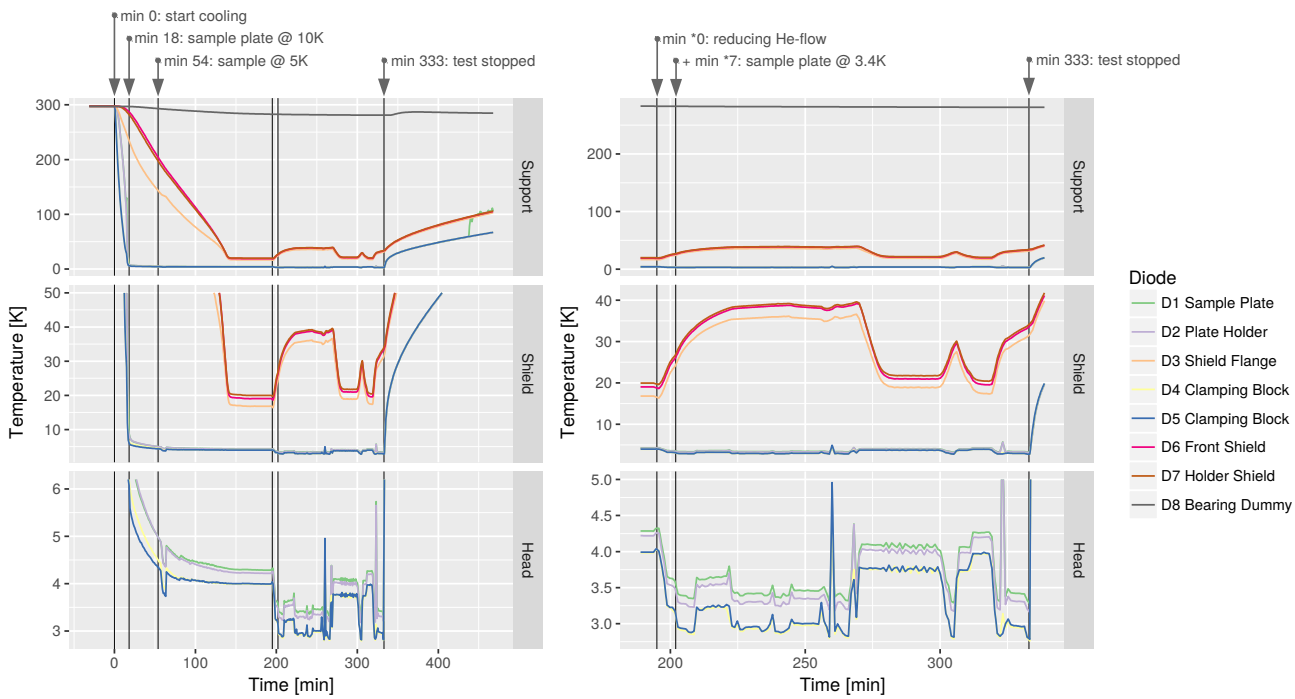

Figure 10: Temperature measurements of the test run.

ISBN: 978-3-95450-207-3 doi:10.18429/JACoW-MEDSI2018-WEOPMA07

REFERENCES

[1] A. Damascelli, "Probing the Electronic Structure of Complex Systems by ARPES", *Physica Scripta*, vol. 2004, no. T109, p. 61, 2004

[2] S. Borisenko, "'One Cubed' ARPES User Facility at BESSY II", *Synchrotron Radiation News*, vol. 25, no. 5, p. 6-11, 2012

[3] L. J. Salerno, and P. Kittel, "Thermal Contact Conductance" *NASA Technical Memorandum*, vol. 110429, 1997

[4] M. G. Cooper, and B. B. Mikic, "Thermal Contact Conductance" *Int. J. Heat Mass Transfer*, vol. 12, p.279-300, 1968

[5] F. Pobell, *Matter and methods at low temperatures.* Berlin: Springer, 2007.

[6] A. L. Woodcraft, "Recommended values for the thermal conductivity of aluminium of different purities in the cryogenic to room temperature range, and comparison with copper", *Cryogenics*, vol. 45, no. 9, p. 626-635, 2005

[7] A. L. Woodcraft, and A. Gray, "A low temperature thermal conductivity database" in *Proc. Aip conference proceedings*, vol. 1185, no. 1, pp. 681-684. AIP, 2009